# Regimes for Conditionally Unstable Flow over an Idealised Three-Dimensional Mesoscale Mountain

S.-H. Chen
National Center for Atmospheric Research, Boulder, CO 80305-3000, USA
Y.-L. Lin
North Carolina State University, Raleigh, NC 27695-8208, USA

## 1. Introduction

Heavy orographic rainfall may occur on the windward slope, upstream, or over the lee slope of a mesoscale mountain range. In studying conditionally unstable flow over an idealized two-dimensional mesoscale mountain, Chu and Lin (2000) identified three moist flow regimes, which are controlled by the moist Froude number defined as $V / N_w h$. In this paper, we make idealized three-dimensional numerical experiments to help identify the moist flow regimes and understand the dynamics.

## 2. Model Description and Experiment Design

The Weather Research and Forecast (WRF) model (Klemp et al. 2001), which has been developed by several institutions, is adopted for this study. The WRF model has the following characteristics: (1) fully compressibile, (2) nonhydrostatic, (3) governing equations in flux form, (4) Klemp-Wilhelmson's time split expicit scheme, (5) Arakawa-C grid, (6) $s - z$ coordinate, (7) free-slip lower boundary condition, (8) rigid upper boundary condition. The options of the open lateral boundary condition, Kain-Fritsch cumulus parameterization, and Lin-Farley-Orville microphysics parameterization are chosen in this study. Detailed information about this model may be found in the website: www.wrf-model.org.

Weisman and Klemp's sounding is used in this study, except that the wind profile is modified to be uniform. The numerical experiments are summarized in Table 1. Both ridge-like and arc-shaped orographies are used. The ridge-like orography has an east-west length of 700 km, and a north-south width of 400 km, which decreases from the ridge line by a square cosine function. The parameters $h$, $a$ (half width), and $\Delta$x (= $\Delta$y) used in the numerical experiments are 2 km, 100 km, and 30 km. The vertical grid interval is stretched from 200 m at the lowest level to 800 m near the domain top. The domain grid points are 111×111×58 in *x-y-z* direction. A 5-km sponge layer is imposed on top of the physical domain (25 km) to absorb waves. The time interval is 120 s, and the nondimensional integration time (*tV/a*) is set to be 4.32.

*Corresponding author address:* Dr. Shu-hua Chen, National Center for Atmospheric Research, Boulder, CO 80305-3000.

## 3. Moist Flow Regimes and Dynamics

a. Flow regimes

Figure 1 shows the accumulated precipitation at $tV/a = 4.32$ for Case 1 ($V = 7.5$ ms$^{-1}$; $F_w = 0.425$). The precipitation area is heart-shaped and it wraps around the mountain (Fig. 1a). The upstream portion has extended to about 1000 km from the mountain ridgeline with the maximum rainfall of over 40 mm located in the 400 km band from the foothill. There is almost no rainfall over the upslope. Although no lee vortices are generated, the convergence on the lee side is still able to trigger convection. The rainfall spreading is associated with the propagation of the convective systems, which is clearly shown in the w field (Fig. 1b]. There exists a stagnation point upstream of the mountain due to strong blocking by the mountain. The maximum upward velocity is located on the upstream side of the mountain.

The heart--shaped convective line is similar to the rainband observed in Hawaii under low-Froude number. In the beginning, the convection is generated over the upslope, which is then propagating upstream associated with the density current (Fig. 1c). Similar to 2D flow (Chu and Lin 2000), the convergence at the gust front is able to trigger new convection. The flow splitting can also be seen from the streamline field (Fig. 1b), while a significant amount of flow is blocked upstream by the mountain. The upward motion located at the northern edge of the lee (north) side cold pool (Fig. 1c) appears to be produced by the convergence associated with the return flows from the eastern and western flanks, and the downslope wind (Fig. 1b). This flow may be characterized as a *regime with upstream-propagating convective systems and return flow generated lee convective systems (Regime I).*

When $F_w$ increases from 0.425 to 0.85 (Case 2), the upstream convective system becomes quasi-stationary (Figs. 2a and b). The maximum rainfall region is confined in a much narrower band, about 200-km wide, just upstream of the mountain range, compared with the lower-$F_w$ case (Fig. 1a). The upstream maximum rainfall is more than 40 mm at $tV/a = 4.32$ (t=8 h). The precipitation pattern and the upward motion region are arc-shaped with the arms extending to the lee side.

However, they do not extend as far as that in Case 1. The stronger basic wind prevents the generation of strong convergence zones on the lee side to trigger convective lines to wrap around the lee side of the mountain (Fig. 2b), as those in Case 1 (Fig. 1b). However, the flow on the lee side does converge toward the centerline. The quasi-stationary behavior of the upslope convective system is well depicted by the vertical cross section along $x = 0$ km (Fig. 2c). The upslope density current is much shallower than that in Case 1 (Fig. 1c). In addition to the major convective system over the upslope, there exists a weaker convective system located over the lee slope. A strong downslope wind is blowing down the lee slope. The weaker convective system over the lee slope appears to be generated by the quasi-stationary hydraulic jump. This flow regime may be characterized as a *regime with quasi-stationary upslope convective system (Regime II).* In this flow regime, the quasi-stationary convective system may be able to produce heavy upslope rainfall. The difference of this flow regime from that found in a 2D flow by Chu and Lin (2000) is that the heavy rainfall is located over upslope, instead of over the mountain peak, and, more importantly, under a low-level jet. This result is more consistent with observations.

When $F_w$ increases further to 1.70, the flow behaves very differently. The nondimensional time is still kept at 4.32, which corresponds to t=4 h. First, the upslope convective system is weaker than that in Case 2, which can be seen from the precipitation amount, i.e. 40 mm in Case 3 and 60 mm in Case 2. Even though the upward motion is stronger in this case, the convection is weakened by the strong advection. Second, a strong convective system downstream is produced (Figs. 3a and b), which is produced by the strong hydraulic jump associated with severe downslope wind (Fig. 3c). Third, unlike previous cases (Figs. 1a and 2a), the convergence on the lee side produced by the flow passing from the eastern and western flanks is too weak to trigger new convection far downstream (Fig. 3a). This flow may be characterized as a *regime with upslope and downslope convective systems (Regime III).*

b. Effects of mountain geometry

Many heavy orographic rain events occurred over the Alps starting near the Ticcino and Lago Maggiore regions, which are near the concave region of the southern Alpine mountains and under the southerly or southeasterly low-level flow. Similar phenomenon also occurred in heavy orographic rain events in other mountain ranges, such as Taiwan's Central Mountain Range. With a horizontal LLJ from south, Schneidereit and Schär (2000) showed that the flow is able to transit from a regime of go-around the mountain to a regime of go-over the mountain if the east-west mountain barrier has a western flank. In addition, the maximum rainfall region is sensitive to the horizontal LLJ location.

In Case 2A, we add a western flank, similar to that in Schneidereit and Schär, but with a uniform southerly wind. Fig. 4a shows the total rainfall at $tV/a = 4.32$. The precipitation pattern is concentrated along the southern slopes. The maximum rainfall is about 60 mm, which is comparable to Case 2. Note that the rainfall does not start at the concave region and has its maximum located slightly to the east. The flow near the concave region has an eastward component, which tends to advect the convective system away from it. The flow behavior on the cross section of x=0 km (Fig. 4c) is similar to Case 2 (Fig. 2c). The resolvable rainfall has a much higher value than that in Case 2 and located slightly to the east of the concave region. The maximum upward motion starts near the concave region and then propagates eastward (Figs. 4b and c). It appears that the microphysical processes are able to react more directly to the upward motion, while the parameterized convection is more sensitive to the horizontal divergence/convergence. In order to have the maximum rainfall located near the concave region, it may require an easterly component.

**4. Concluding Remarks**

Three flow regimes are identified for a conditionally unstable flow over a three-dimensional mountain range: (I) regime with upstream-propagating convective systems and return flow generated lee convective systems, (II) regime with quasi-stationary upslope convective system, and (III) regime with upslope and downslope convective systems. The major differences from the same flow over a two-dimensional mountain range are: (1) flows are allowed to go around the mountain, which helps to produce convective lines moving outward on the upstream side of the mountain and curve into the mountain on the lee side, (2) maximum rainfall is produced at Regime II and is located over the upslope, instead of over the mountain peak, (3) heavy upslope rainfall can be produced under a LLJ, (4) the strength of the upslope convection is not necessarily proportional to the basic wind speed since it may be weakened by the basic wind advection. With a concave geometry, we found that the unresolvable rainfall has its maximum located to the southern sides of the major mountain barrier and the western flank, while a significant amount of resolvable rainfall is produced near the concave region. In order to have the maximum rainfall located near the concave region, it may require an easterly component.

**Acknowledgements:** This work is supported by NSF Grant ATM-0096876 and Air Force Weather Agency. The authors would like to thank the WRF team for their efforts in developing the WRF model.

**References**

Chu, C.-M., and Y.-L. Lin, 2000: Effects of orography on the generation and propagation of mesoscale convective systems in a two-dimensional conditionally unstable flow. JAS, **57**, 3817-3837.

Klemp, J. B., and W. C. Skamarock, and J. Dudhia, 2001: Prototypes for the WRF (Weather Research and Forecast] model. 9th Conf. Meso. Processes, AMS (also see www.wrf-model.org)

Schneidereit, M., and C. Schär, 2000: Indealised numerical experiments of Alpine flow regimes and southside precipitation events. Meteor. Atmos. Phys., 72, 233-250.

**Table 1.** Characteristics of the Numerical Experiments

| Case | V | $F_w$ | Integration Time (h) | Flow Regime | Upstream/upslope/downstream convective systems |
|---|---|---|---|---|---|
| 1 | 7.5 | 0.425 | 16 | I | Yes/no/yes |
| 2 | 15.0 | 0.850 | 8 | II | No/yes/no |
| 3 | 30.0 | 1.700 | 4 | III | No/yes/yes |
| 2A** | 15.0 | 0.850 | 8 | II | No/yes/no |

* $N_w = 0.006$ s$^{-1}$, $h = 2$ *km*, $a =$ 100 km, CAPE = 2049 $J\,s^{-1}$; **Case 2A is with an arc-shaped mountain.

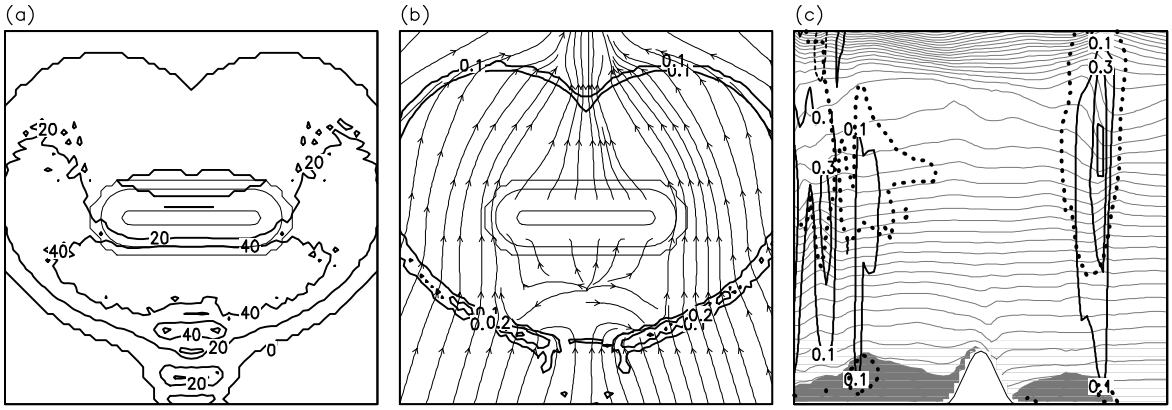


Fig. 1: (Case 1) (a) The surface accumulated precipitation (mm) (thick lines), (2) w ($\mathrm{ms}^{-1}$) (thick lines) and streamlines at z=1000 m, and (c) w ($\mathrm{ms}^{-1}$) (thick lines) along x=0 km and $q$ (thin lines) after 16-h (Vt/a=4.32) simulation. The topography is plotted in (a) and (b) with thin solid lines. In (c), the thick dotted line denotes the total water content of 0.1 $\mathrm{g\,kg}^{-1}$ and $q' < 1K$ is shaded. The plotting domain is (2010, 2010, 14km).

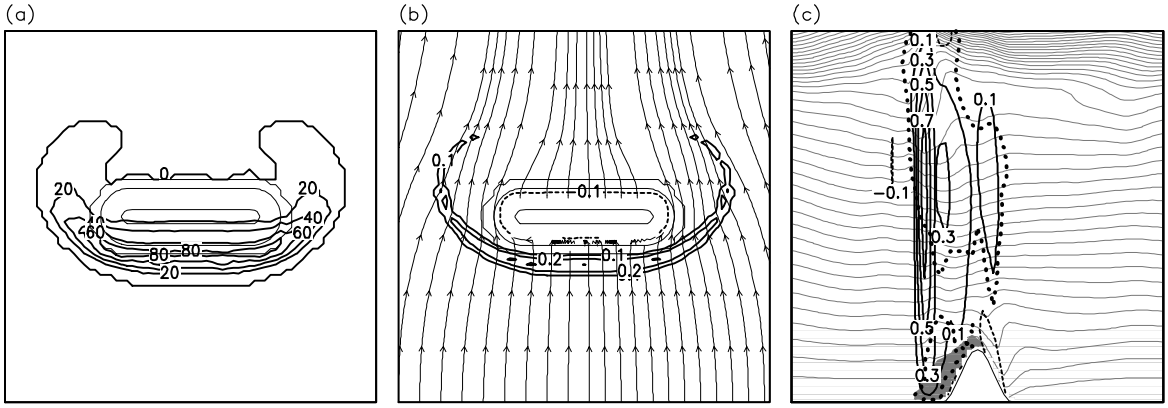


Fig. 2: Same as Fig. 1 except for Case 2.

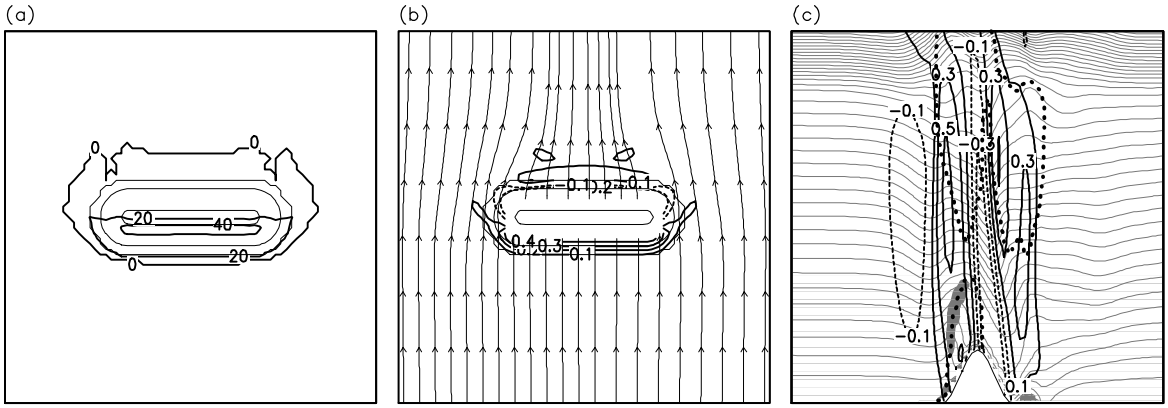


Fig. 3: Same as Fig. 1, except for Case 3.

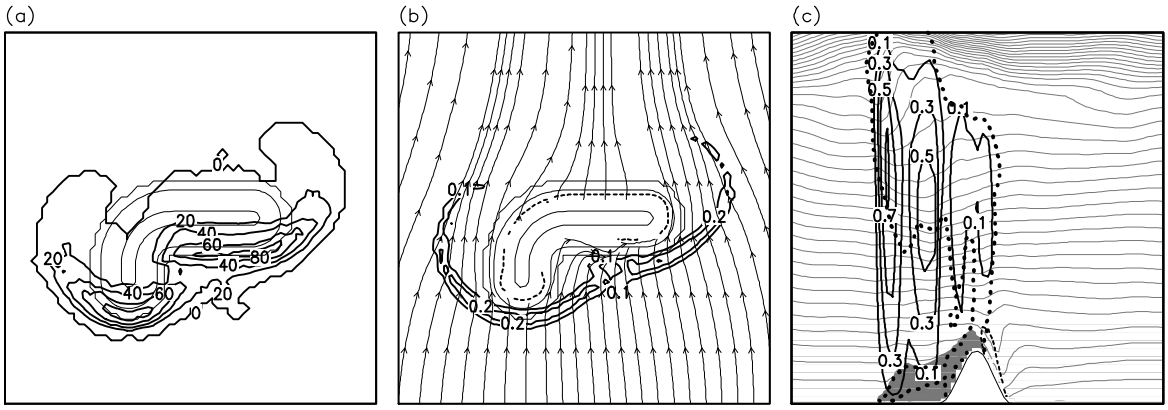


Fig. 4: Same as Fig. 1, except for Case 2A and panel c is along x = - 60 km.